RESEARCH ARTICLE

VOLCANICA

First hydroacoustic recording of mass bubbling events in an active volcanic lake – Poás, Costa Rica

Ben Roche*[α], Corentin Caudron[α], Leonardo van der Laat[β], J. Maarten de Moor[β,γ], Geoffroy Avard[β], Javier Pacheco[β], Henriette Bakkar[β], Julien Govoorts[α], and Alejandro Rodriguez[β]

[α]Université libre de Bruxelles, Avenue Franklin Roosevelt 50, 1050 Brussels, Belgium.
[β]Observatorio Vulcanológico y Sismológico de Costa Rica, Universidad Nacional (OVSICORI-UNA), Costa Rica.
[γ]Department of Earth and Planetary Sciences, University of New Mexico, Albuquerque, NM, USA.

Abstract

This study demonstrates how the sounds of subaqueous gas seeps can be used to measure the volume of volcanic gas being released into an active crater lake, weeks before an eruptive period. A hydrophone placed in Poás crater lake recorded changes in the subaqueous soundscape over the course of one month. Using new passive acoustic inversion techniques, we were able to measure the volume of gas being released from the lakebed at a sample rate of 5 min, far higher than traditional sub aerial gas sampling techniques. Comparing these findings to local seismic measurements allowed us to observe variations in gas flux driven by both volcanic and non-volcanic factors. Non-volcanic causes consist of small-scale diurnal variations of ~2 L min^{-1} driven by local atmospheric pressure conditions. We also see a large and abrupt aseismic mass bubbling event releasing 18,000 ± 3000 L of gas in just 15 hours (compared to a daily average of 3600 ± 500 L) likely resulting from the collapse of gas pocket(s) in the sediment underlying the lake. Alongside an even larger mass bubbling event releasing 30,000 ± 5000 L of gas in 24 hours correlated with local seismic activity, presumed to be triggered by excess volatiles being released from deeper within the volcano, which preceded a new eruptive period at Poás volcano. This work paves the way for future studies to quantify subaqueous volcanic gas emissions via hydroacoustics, a potential new volcano monitoring technique.

Keywords: Active volcanoes; Monitoring techniques; Bubbles; Hydroacoustic; Phreatic eruption; Degassing.

Submitted: 2024-08-22 | Accepted: 2025-01-29 | Published: 2025-04-15

Editor: J. Farquharson | Typesetter: J. Farquharson

1 Introduction

Volcanic degassing is a well-known phenomenon, with H_2O, CO_2, SO_2 and other gases rising from magma reservoirs in the crust to the surface through various conduits and cracks [Chiodini et al. 2016; Longo et al. 2021]. A correlation between the level of volcanic activity and degassing has long been noted but is yet to be empirically quantified [Vandemeulebrouck et al. 2000; Caliro et al. 2004; Caudron et al. 2012; Chiodini et al. 2016; Longo et al. 2021; Caudron et al. 2022]. This is because accurately measuring the volume of gas released from a volcano is extremely difficult. Subaerial gas vents (fumaroles) are often easy to locate but can be challenging or impossible to sample. Though gas monitoring techniques such as Multi-GAS greatly improve the sample rate of atmospheric gas measurements and show promise for eruption forecasting [de Moor et al. 2019], gas data acquisition still does not compare with the sample rate of seismic data, typically only providing a couple of measurements a day compared to sampling at frequencies of ~100 Hz [de Moor et al. 2019]. The issue is further complicated when hazardous gases are involved, which bring additional safety concerns. Subaqueous gas seeps on the other hand are generally safe and easy to locate, with bubble plumes being easily identifiable in the water column and often even at the water's surface. Nevertheless, they are still difficult to physically sample [Leifer and Patro 2002; McGinnis et al. 2006]. Thus, subaqueous volcanic degassing is relatively underutilized in volcanic monitoring.

Please note to avoid confusion in this paper we will refer to subaerial gas vents as "fumaroles" and subaqueous gas vents as "seeps." This is keeping in line with bubble acoustic literature which commonly refers to sea floor vent sites as "seeps" and "seep fields" [Roche 2023].

While there are a variety of techniques researchers can use to quantify subaqueous gas emissions, many of these are severely limited in terms of temporal coverage, sample rate, and cost [Etiope and Schwietzke 2019]. Physically measuring the gas flux—i.e. recording how long it takes to displace a known volume of water—is still commonly used. Such work can be done with divers or automated landers [Tokoro et al. 2007; Zhu et al. 2010; Maeck et al. 2014; Mannich et al. 2019]. However, such systems are bespoke, are restricted to lower flux seeps, have a limited sampling rate, and perturb the natural fluid flow. Optical measuring techniques are far less intrusive but are limited in the area they can survey, being dependent on water visibility (which can be near zero depending on the study area) and the size of the gas bubbles [Makarov et al. 2020; Razaz et al. 2020; Li et al. 2021; Veloso-Alarcón et al. 2022]. Moreover, they are unlikely to cope well with acidic conditions encountered in active volcanic lakes. Active acoustic measurement techniques (both multi- and single-beam based), while being able to cover a large area, are expensive and require time-consuming processing to produce accurate quantitative data and hence typically only provide a snapshot measurement [Veloso et al. 2019; Urban et al. 2023]. Furthermore, the accuracy of the assumptions that underpin the conversion of active acoustic data into gas

*ben.john.roche@ulb.be

fluxes is still evolving [Li et al. 2020b; Urban et al. 2023]. However, hydroacoustics—studying the sounds produced by a gas seep within the water column using hydrophones—is a low energy technique, capable of long-term deployments in any level of visibility, with a high sampling rate (e.g. 5 minutes as seen in this study), and minimal perturbation of the seeps [Leighton and White 2011; Bergès et al. 2015; Vazquez et al. 2015; Haris et al. 2023].

Previous attempts at using hydroacoustics to study volcanic gas emissions have focused either on individual bubble emissions or on recording the intensity of sound at set frequency bands with increase in acoustic volume/intensity acting as a proxy for increase in gas flux [Vandemeulebrouck et al. 2000; Longo et al. 2021; Caudron et al. 2022]. The latter is an incredibly useful first order approximation and has proven successful in demonstrating a link between subaqueous gas flux and volcanic activity [Longo et al. 2021]. However, it is underpinned by the rarely correct assumption that all the sound recorded by the observer is a result of the gas seep [Longo et al. 2021] whereas subaquatic settings are complex acoustic environments with numerous sound sources [Bayrakci and Klingelhoefer 2023]. Furthermore, this approach does not account for the fact that the released bubble size population is not fixed in time and likely varies; such small changes are easily missed between large frequency bands. Most importantly, these approaches have failed to quantify the gas flux itself [Vandemeulebrouck et al. 2000; Longo et al. 2021]. We propose a solution to this problem with a new passive acoustic flux inversion technique, analysing a wider frequency band to estimate the volume of gas released over an extended period of time.

Passive acoustic flux inversion relies on a physical model of the sound emitted by a bubble as it is released into the water column. The moment a bubble is released a volume oscillation is triggered. The frequency of this oscillation (f_M) is inversely proportional to the equilibrium radius of the bubble (R_0) as described by the Minnaert equation below [Leighton 1994]:

$$f_M = \frac{1}{2\pi R_0}\sqrt{\frac{3k p_0}{\rho}}, \tag{1}$$

where is ρ is the density of water, p_0 is the hydrostatic liquid pressure outside the bubble, and k is the polytropic index [Roche 2023]. Hence, by observing the frequency of a bubble one can determine the volume of gas within it [Leighton 1994]. Note that the gas content has no perceivable effect on the frequency of a bubble's oscillation. Thus, determining the size of a single bubble oscillating in a quiet environment is computationally trivial. In higher flux situations characterized by many bubbles being released at the same time, one cannot differentiate individual bubble signals and must instead consider the spectral density of the acoustic pressure released from the seep as perceived by a hydrophone in the far-field [Leighton and White 2011]. Using a model of the spectrum of the signature of each bubble formation event, the measured spectrum can be used to infer the bubble size distribution. By knowing the distance between the seep and the recording hydrophone, the number of bubbles of any given size that are released within a given time window/sample period (e.g. 300 s) can be inferred. This can be used to calculate the total volume of gas in said period and thus retrieve the gas flux [Leighton and White 2011; Bayrakci and Klingelhoefer 2023].This technique has been successfully demonstrated in a range of environments from test tanks to Scottish Lochs, German Lakebeds and North Sea pockmarks at rates ranging from 0.1 to 100 $\mathrm{L\,min^{-1}}$ [Bergès et al. 2015; Li et al. 2021; Roche 2021]. In instances when more than one seep is active, i.e. a seep field, the mean distance between the receiver and the surrounding seeps must be used, the assumption being that the rate of over estimation caused by seeps closer than the receiver is countered by underestimation of those further away. The maximum range across which inversion can be performed is still being investigated and is likely principally dependent on the background noise levels in the site. In shallows coastal waters a detection range of 25 m has been demonstrated [Haris et al. 2023], meaning an even greater range is likely in quiet, isolated environments.

This study analyses hydroacoustic data recorded by a single hydrophone in the warm hyperacid crater lake atop Poás Volcano (Costa Rica) in June 2023. We quantify the gas flux from subaqueous seeps in this highly active volcanic lake at a sample rate of 5 min, far greater than traditional subaerial sampling techniques, using passive acoustic flux inversion techniques. This allows us to observe both small scale diurnal variations driven by local atmospheric pressure conditions and large abrupt changes correlated with changes in local seismic activity and subaerial volcanic gas levels. This study demonstrates the potential for hydroacoustics as a volcanic monitoring technique, potentially providing improved knowledge of volcanic systems.

1.1 Study area: Poás Crater Lake

Poás volcano is an active stratovolcano located in central Costa Rica. Located at the summit is an ephemeral acidic hot crater lake, alongside a number of subaerial fumaroles (Figure 1) [de Moor et al. 2016]. The dimensions and level of the lake varies with rainfall and volcanic activity. At the time of our experiment, it was ~2 m deep with a diameter of ~300 m (Figure 1) [D'Arcy et al. 2022]. The volcano is characterised by cycles of phreatic and phreatomagmatic activity [D'Arcy et al. 2022]. Notably, an extended period of phreatic activity began in 2006 and culminated in 2014 with series of phreatic blasts, ~300 m high, centred in the crater lake prompting increased interest in monitoring the site. This was followed by a short period of phreatomagmatic activity in 2017 and more phreatic activity in later 2017 to 2019 [de Moor et al. 2016; Salvage et al. 2018]. After the conclusion of survey described in this study a new period of phreatic activity was reported between July 21st 2023 and May 28th 2024 (see Figure 1).

Unpredictable frequent phreatic eruptions are of concern given that the volcano is visited by more than 200,000 tourists a year. Phreatic eruptions are notoriously difficult to predict as they often do not involve the movement of magma, meaning there can be no clear warning signals [Rouwet et al. 2014; de Moor et al. 2016]. Atmospheric measurements show an average SO_2 flux of ~150 $\mathrm{T\,d^{-1}}$ between 2019 and 2024 [de Moor et al. 2016; D'Arcy et al. 2022]. Studies have also con-

cluded volatiles from the fumaroles and above the lake have a common source [Rouwet et al. 2014; de Moor et al. 2016]. These magmatic volatiles are released directly into the lake through various seeps, hence increases in the amount of bubbling could precede phreatic eruptions. Such changes should be identifiable and quantifiable with hydroacoustic monitoring at much higher time resolution than traditional geochemical monitoring techniques.

2 Methods and materials

2.1 Data acquisition

For this study a Snap hydrophone with a sensitivity of −170 dBV/µPa was used. It was placed at the eastern lake edge 30 m from a known seep field (Figure 1). It was deployed horizontally on the lakebed at a water depth of 2 m (as measured at the time of deployment) being secured in place by ropes tied to nearby rocks. It recorded at a sample rate of 8000 Hz resulting in a workable frequency range of 10 to 8000 Hz. The hydroacoustic data used in this study was collected continuously between the 3 and 27th of June, totalling 600 hours of audio data.

Seismic data was collected during the same period at a sample rate of 100 Hz using the local network of broadband stations. We show data for the vertical component of the closest station to the crater located ~400 m SE of the hydrophone (Figure 1), VPCR, which includes a Kinemetrics 120 s broadband sensor (MBB-2).

Gas concentrations (CO_2, SO_2, H_2S) and ratios (SO_2/CO_2, H_2S/SO_2) were monitored during the study period using a permanent MultiGAS station located on the western rim of the crater ~500 m SW of the Hydrophone (Figure 1). The station conducted 3 analysis sessions of 30 min each per day, collecting concentration data at a rate of 0.33 Hz. Data were processed to extract gas ratios using linear regression as described in de Moor et al. [2019].

Meteorological data (rainfall and windspeed) was generously supplied by the Costa Rican Instituto Meteorologico Nacional (IMN) from the nearby Poás–Alajuela weather station located ~1 km south of the crater. All times are given in UTC, which we note is 6 hours ahead of local time.

2.2 Data analysis

2.2.1 *Passive acoustic flux inversion*

Hydroacoustic data was processed using the methodology first laid out by Leighton and White [2011], with further refinements by Roche et al. [2022]. For a complete understanding of the inversion process we refer the reader to these earlier works however the inversion process can be summarised as thus.

1) The recorded acoustic data is broken into a series of smaller sections, in this case 5 min long, this ultimately determines the sample rate of flux measurements.

Then for each acoustic section

2) The acoustic spectrum is split into equally sized frequency bands between a set minimum and maximum frequency (1600 and 4000 Hz here). Each frequency band correlates to bubble radius via Equation 1;

3) The total energy recorded within each frequency band is then determined before an average per second value is calculated;

4) The number of bubbles of the corresponding radius that would need to be released per second to match the observed energy at a specified distance is then calculated by the model (using equations laid out in Leighton and White [2011]) for each frequency band;

5) The result is a list of the number of bubbles of varying radii released per second in the inverted time section. Extrapolating this out gives the total number of bubbles of varying radii released in the time section. Multiplying the volume of each of these bubble radii by the total number of bubbles ultimately provides the total emission in liters per time section, most easily presented in $L\,min^{-1}$.

The acoustic data was first manually interrogated to identify which frequency range represents bubble emissions (i.e. a researcher listened to isolated frequency bands throughout the survey period and judged whether or not they could hear bubbles). Ultimately this was identified as being between 1600 and 4000 Hz (see Results), corresponding to bubbles with an equilibrium radius between 2.2 and 0.9 mm. Sub 1600 Hz signals were avoided as the spectrum was dominated by non-bubble sounds, most notably the roaring of the subaerial fumaroles. While ideally, we would like to be able to record bubble signals below 1600 Hz this problem is insurmountable. This is because bubbles with a radius larger than 5.0 mm (with a frequency of ~700 Hz) are less common in shallow waters (<3 m deep), as such a gas volume greatly exceeds the buoyancy force typically needed to escape the upper sediment [Leighton 1994; Roche 2023]. Furthermore, larger bubbles are significantly more likely to break apart than smaller ones, with the resulting daughter bubbles oscillating in the same manner as the parents, with the volume of the parent bubble matching the total sum of the daughter bubbles [Martínez-Bazán et al. 1999; Deane and Stokes 2008; Qi et al. 2020]. Hence, while a number of bubbles with radii between 2.2 and 5.0 mm may be released, subsequent break-up means that their volume will ultimately be included in the total emissions [Roche et al. 2022]. Regardless, this study focuses more on the relative changes in gas flux rather than attempting to measure the exact volume of gas flux in the whole lake, which is not possible with a single hydrophone.

Typically, in order to perform acoustic inversion, the distance between the hydrophone and the gas seep needs to be known. In Lake Poás the gas release is not restricted to a single seep but rather a number of seep fields, containing multiple seeps with the nearest permanent seep located ~30 m from the hydrophone (Figure 1). The advantage of multiple (near) homogenous sound sources in a field in shallow water is the that we can assume the constructive interference of indirect sound waves from one source, as a result of the Lloyd's mirror effect, is counted by the constructive interference of indirect waves from another [Li et al. 2020a]. It has been demonstrated

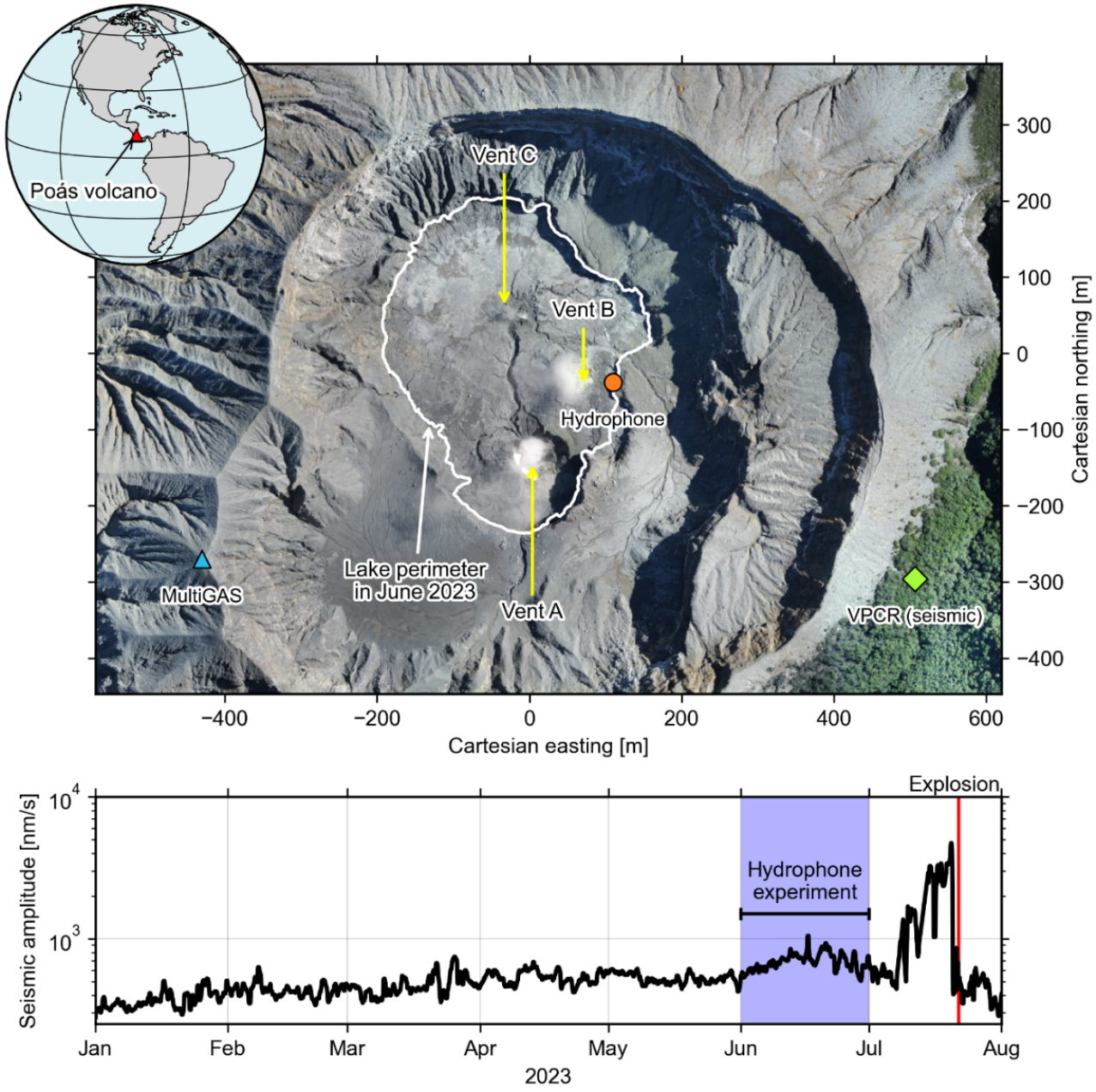

Figure 1: Overview of Area of study and recent seismic activity. [Top] Overview of Poás Crater. Image is an ortho-mosaic from 2019 when the lake was dry. The 2023 lake perimeter during the time of study is shown in white. The location of the hydrophone is shown in orange, alongside the MultiGAS (blue) and seismic (green) sensors. Note the relative distance to the persistent vents. [Bottom] graph of seismic amplitude (smoothed using a 12 hour median: see methodology for more details) in the months surrounding the study period. Note the large increase and explosion in the following month.

in shallow water that the attenuation of bubble signals makes detection beyond 25 m difficult [Haris et al. 2023]. Thus this study has elected to use an inversion range of 25 m as it is a proven inversion range. Note this does not mean we are insensitive to the flux from seeps at a greater distance, simply that their relative contribution becomes increasingly underestimated with distance from this point, making the effective range less than 50 m. Consequently, the resulting values will represent the minimum rate of emissions from the nearest seeps and not the lake as a whole. The largest source of error in passive acoustic flux inversion process arises from uncertainties in the ration of the initial radius of excitation of a bubble to its equilibrium radius. This ultimately results in an error of ±15 % [Roche et al. 2022]. A full list of the inversion settings can be found in Supplementary Material 1 Table S1.

It should be noted that the rate of gas release from submarine seeps can vary for a number of reasons. While this study is focused on changes driven by magmatic-hydrothermal sources, natural gas seeps are often regulated by the tidal cycle (high tide resulting in decreased flux rates) and in areas

with little tidal variation even small changes in atmospheric pressure can have an effect (increases in atmospheric pressure resulting in decreased flux rates) [Tokida et al. 2007; Roche 2021]. It is thus important that any study of volcanic gas seeps attempts to distinguish between fluctuations in flux driven by magmatic-hydrothermal activity versus other sources (e.g. tidal change). Furthermore, it is possible for high winds (>30 km hr^{-1}) and rainfall (>5 mm hr^{-1}) to form bubbles at the water's surface [Nystuen 1986; Wang et al. 2016; Roche 2023] which, if not properly provenanced, could be falsely attributed to volcanic seeps. Hence it is also important for studies to be aware of weather conditions throughout their observations.

The final output of the inversion process is a continuous measurement of the gas flux and bubble population size from the adjacent seep field in 5-minute increments. Any increment which showed more than a 25 % change from a previous increment was flagged for manual inspection. If upon review it was found to contain non bubble noise, i.e. the sound of the cable clanging (see supmat1 Figure S1), the value was not included in the final results. The results are presented as a 3 hour running mean throughout the period of observation. Values are quoted to 2 significant figures with an error of ± 15% to a minimum value of ± 0.1 L min^{-1}.

2.2.2 *Hydroacoustic intensity data*

In order to compare results to previous work this study replicates the approach used by prior researchers, measuring the intensity of sound at set frequency bands [Vandemeulebrouck et al. 2000; Longo et al. 2021]. Frequency bands were selected to represent the range of data record and correspond with subsequent passive acoustic inversion inputs: 100–200, 400–600, 800–1000, 1000–1200, 1600–1800, 2000–2600 and 3000–4000 Hz. Note that these bands have no effect on the inversion process, they are merely used to give the reader a broad understanding of the marine soundscape in the lake.

2.2.3 *Seismic data*

The median seismic amplitude from the vertical component of VPCR station is calculated by first pre-processing the data through detrending, scaling to nanometers per second (nm s^{-1}), decimating to 50 Hz, and filtering between 1 and 24 Hz. The processed data is then squared, and the median of these squared values is computed. Subsequently, the square root of this median is taken. This procedure is applied using a 120-second moving window with a 50 % overlap. Data is further post-processed by taking the median in longer moving windows, i.e. 1 h and 12 h.

2.2.4 *Meteorological data*

Data from the nearby Poás–Alajuela weather station was used to identify periods where high wind (>30 km hr^{-1}) and rainfall (>5 mm hr^{-1}) may have resulted in non-volcanic bubbles forming on the water's surface (i.e. noise) and subsequently exclude them from the inversion process. We note the weather station is located outside of the volcanic crater and therefore does not represent an exact match for conditions at the lake but should still serve as a useful indication. All data was received directly from the Costa Rican Instituto Meteorologico Nacional (IMN) and is displayed raw.

3 Results

Observations from June 3rd to June 27th, 2023, are presented in Figure 2, showing the acoustic gas flux measurements, the seismic amplitude, acoustic band data and the subaerial gas measurements. The observations can be divided into three sections: the steady-state period, the mass bubbling period and post mass bubbling period. The steady-state period occurred between June 3rd and 13th, the mass bubbling period occurring between June 13–19th and the post mass bubbling period occurring from the 19th onwards. We present each in order.

3.1 Steady-state period

An example of a 24-hour period during the steady-state period is shown in Figure 3 with an example of the acoustic data available in Supplementary Material 1 Figure S2. Most intensity bands remain constant but there is a decrease in the intensity of 1600–1800 Hz band during the mid portion of the day (Figure 3A). This decrease begins at around 00:00 UTC, flattening out at around 08:00 UTC before beginning to increase again at 1500 UTC and peaking at 20:00 UTC. Weather data during this period shows only a small period of rainfall between 22:00 and 24:00 UTC peaking at 1.2 mm hr^{-1} and windspeeds never exceed 10 km hr^{-1}. They thus are unlikely to have an effect on the subaquatic soundscape.

The flux inversion values for this period vary between 4.0 ± 0.4 L min^{-1} and 1.0 ± 0.1 L min^{-1} (Figure 3A), steadily decreasing from a peak at around 00:00 UTC flatting off at 08:00 UTC before beginning to increase again at 15:00 UTC and peaking at 20:00 UTC. Seismically no discernible trend is visible during this period (Figure 3B). It is not possible to observe a trend in subaerial plume gas compositions due to the low frequency of MultiGAS measurements on this day.

This pattern is repeated throughout the following days (Figure 4). The lower frequency bands (<1500 Hz) during this period show very little variation, remaining fairly stable, whereas the higher frequency 1600 to 1800 Hz and 2000 to 2600 Hz bands continue to show the same diurnal variation. It is notable that the difference between the high frequency bands stays relatively consistent throughout. A series of spikes in the higher frequency bands is also observed and these do correlate with periods of high rainfall (>5 mm hr^{-1}) which were excluded from the inversion process (Supplementary Material 1 Figure S2).

This pattern is also reflected in the gas flux estimates. The flux values range from 6.3 ± 0.9 L min^{-1} to 0.9 ± 0.1 L min^{-1}. On average the range between daily highs and lows is equal to 2 L min^{-1}. In total over the 10-day period the release of 36,000 ± 5,000 L of gas was detected, an average of 2.2 ± 0.3 L min^{-1}.

The seismic data shows no diurnal pattern but a gentle increase over the entire period of 27 %. The average SO_2/CO_2 ratio for this period was 0.91 ± 0.22 and SO_2 concentrations varied from 0 ppm to 21 ppm. The H_2S/SO_2 ratio was close to zero.

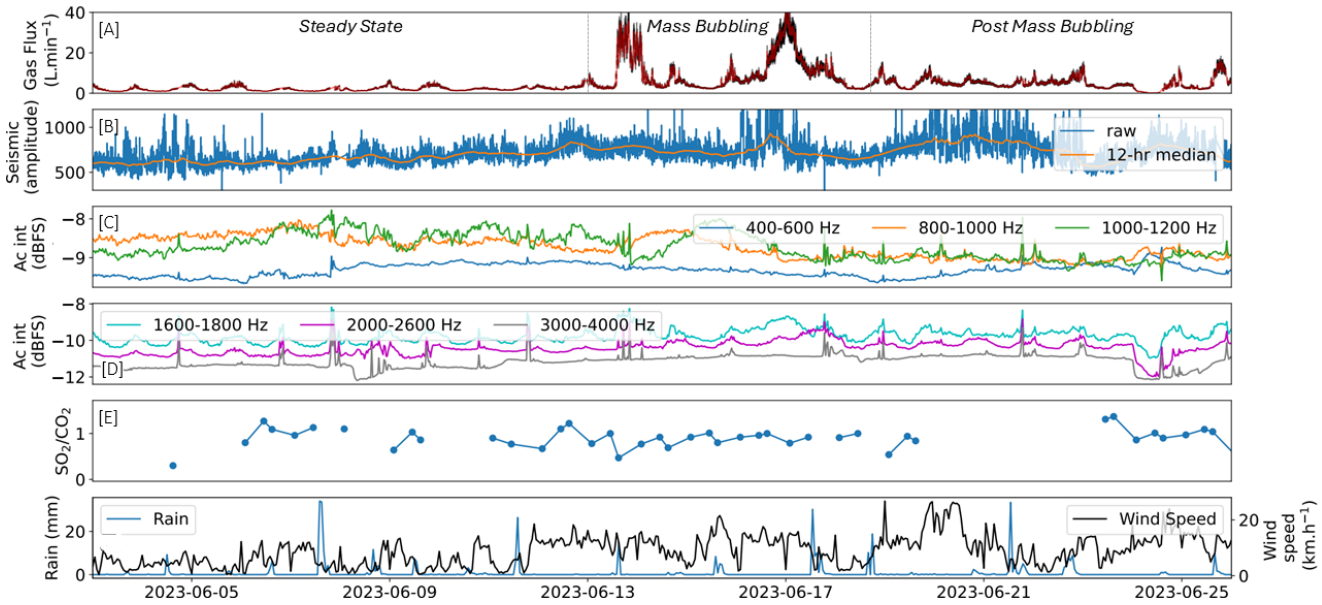

Figure 2: Overview of acoustic, seismic, and chemical results from June 3rd to 27th. [A] The flux inversion results produced based on hydroacoustic data. The red line represents the 3-hour running mean while the black denotes the error. [B] The seismic amplitude recorded at a local station. [C–D] The intensity of different acoustic bands as observed in the lake. Split between low (<1500 Hz) and high frequency (>1500 Hz). The intensity is displayed in dB full scale. Note the spikes in frequency bands correlate with rainfall events and are discounted from flux estimates. [E] Subaerial gas plume SO_2/CO_2 mixing ratios from MultiGAS. [F] the local rainfall (blue) and windspeed (black) data.

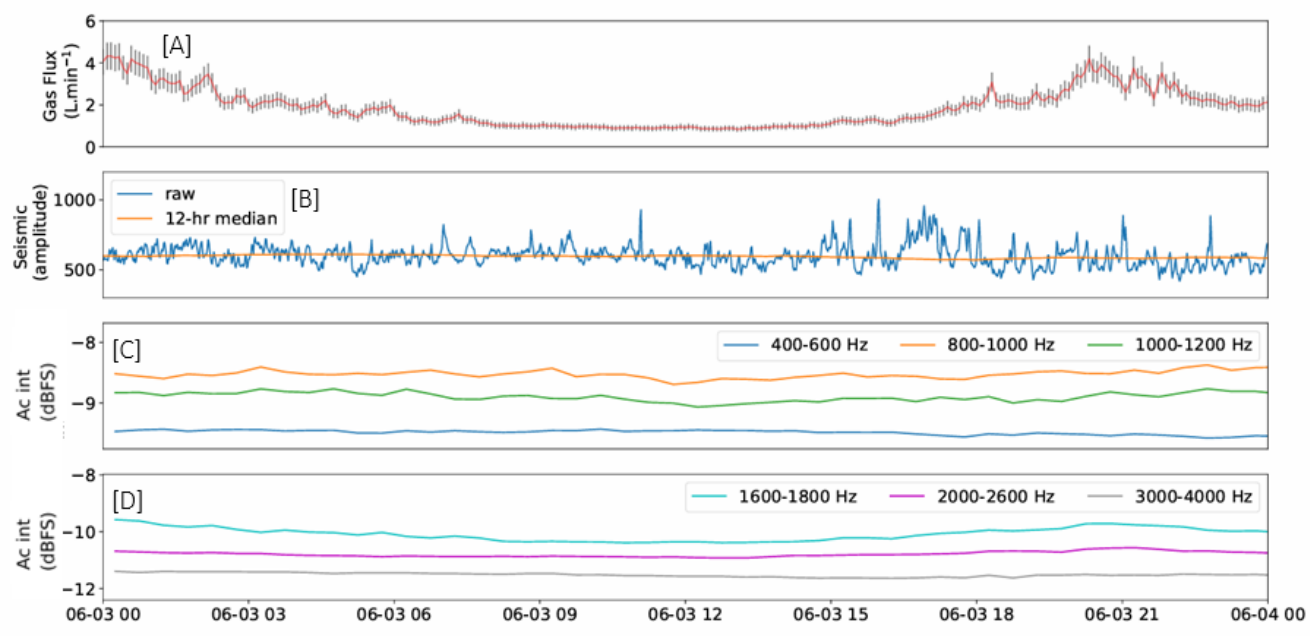

Figure 3: Overview of acoustic and seismic for a single day in the steady-state period observations from June 3rd. [A] The flux inversion results produced based on hydroacoustic data. [B] The seismic amplitude recorded at a local station. [C–D] The intensity of different acoustic bands as observed in the lake. the 10-day period the release of 36,000 ± 5000 L of gas was detected, an average of 2.2 ± 0.3 L min^{-1}. The seismic data shows no diurnal pattern but a gentle in crease over the entire period of 27 %. The average SO_2/CO_2 ratio for this period was 0.91± 0.22 and SO_2 concentrations varied from 0 ppm to 21 ppm. The H_2S/SO_2 ratio was close to zero.

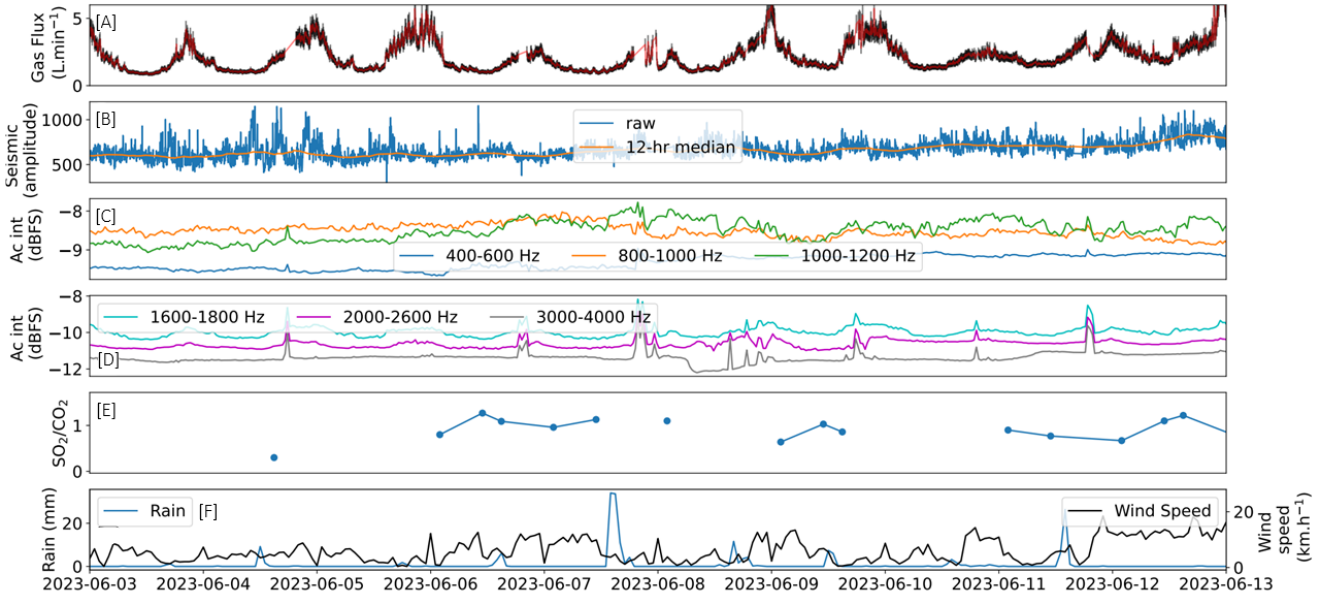

Figure 4: Overview of acoustic, seismic, and chemical results for the steady-state period. Observations from June3rd to13th, the steady-state period. [A] The flux inversion results produced based on hydroacoustic data. Note the daily cycle. [B] The seismic amplitude recorded at a local station. [C–D] The intensity of different acoustic bands as observed in the lake. Spilt split between low (<1500 Hz) and high frequency (>1500 Hz). Note the spikes in frequency bands correlate with rainfall events and are discounted from flux estimates. [E] Subaerial gas plume SO_2/CO_2 mixing ratios from MultiGAS. [F] the local rainfall (blue) and windspeed (black) data.

3.2 Mass Bubbling Period

The mass bubbling period began at approximately 11:00 UTC on June 13th when there was a sharp increase in high frequency signals (>1500 Hz) lasting ~15 hours with a similar increase, but less sudden, occurring again at midday on the 16th lasting nearly 24 hours (Figure 5). This is most clearly seen in the 1600–1800 Hz band (Figure 5C). The 1000–1200 Hz signal during this period initially drops sharply before rising steadily and peaking midway between these two events and returning to prior levels after the 2nd event has concluded. For an example of the acoustic data from each see Supplementary Material 1 Figure S3 and S4.

The first event is reflected by the estimated flux rising from 2.6 ± 0.4 L min^{-1} to 28.0 ± 4.2 L min^{-1} over the course of 3 hours. This increased flux plateaus and continues for approximately 10 hours before rapidly decreasing (over the course of ~3 hours) back down to levels seen during the previous steady state (<5 L min^{-1}) and the diurnal variation cycle seems to resume. The second event sees flux rates rising steadily over 12 hours from 7.7 ± 1.2 L min^{-1} to peak at 49.0 ± 5.0 L min^{-1}. Flux levels then steadily decrease again over another 12 hours to 10.5 ± 1.6 L min^{-1} at which point the diurnal variation cycle returns. The first event saw a total of $18{,}000 \pm 3000$ L of gas released (18 ± 3 L min^{-1}) while the second saw $30{,}000 \pm 5000$ L (21 ± 3L/min). We have thus elected to refer to these events as "mass bubbling events" akin to a kind of bubble eruption.

No high winds were recorded throughout this period. A short period of high rainfall (15.6 mm hr^{-1}) occurred during the first event between 20:00 and 21:00 UTC and can be seen as spikes in the intensity band graphs. No rainfall was recorded during the second event .

Seismic amplitude does not increase during the first event but increases during the onset of the second event with the number of short-tremor events rising above background levels.

MultiGAS data shows that no major changes in the gas emissions occurred during the mass bubbling period compared to the steady-state period. The SO_2/CO_2 ratio averaged 0.86 ± 0.16 and the H_2S/SO_2 remained near zero. The lowest SO_2/CO_2 ratio (0.47 on the 13 June at ~2:45pm) recorded during the mass bubbling period corresponds to the first mass bubbling event and no anomaly was recorded during the second.

3.3 Post-mass bubbling period

Following the last mass bubbling event high frequency signals (>1600 Hz) decrease significantly, though are still more intense than that seen during the steady-state period (Figure 6D). For an example of the acoustic data see Supplementary Material 1 Figure S5. The diurnal variation is still broadly visible though less prominent than before. A notable decrease in intensity is seen at around 02:00 UTC on the 24th followed by a sharp increase at around midday. The low frequency signals (<1200 Hz) remain broadly constant. Gas flux estimates during this period reflect the higher frequency pattern, showing a less consistent diurnal variation, generally ranging between 3 and 11 L min^{-1}, with a notable low of 0.2 ± 0.1 L min^{-1} occurring in the morning of the 24th and a high of 13.0 ± 2.0 L min^{-1} on the 25th at 17:00 UTC.

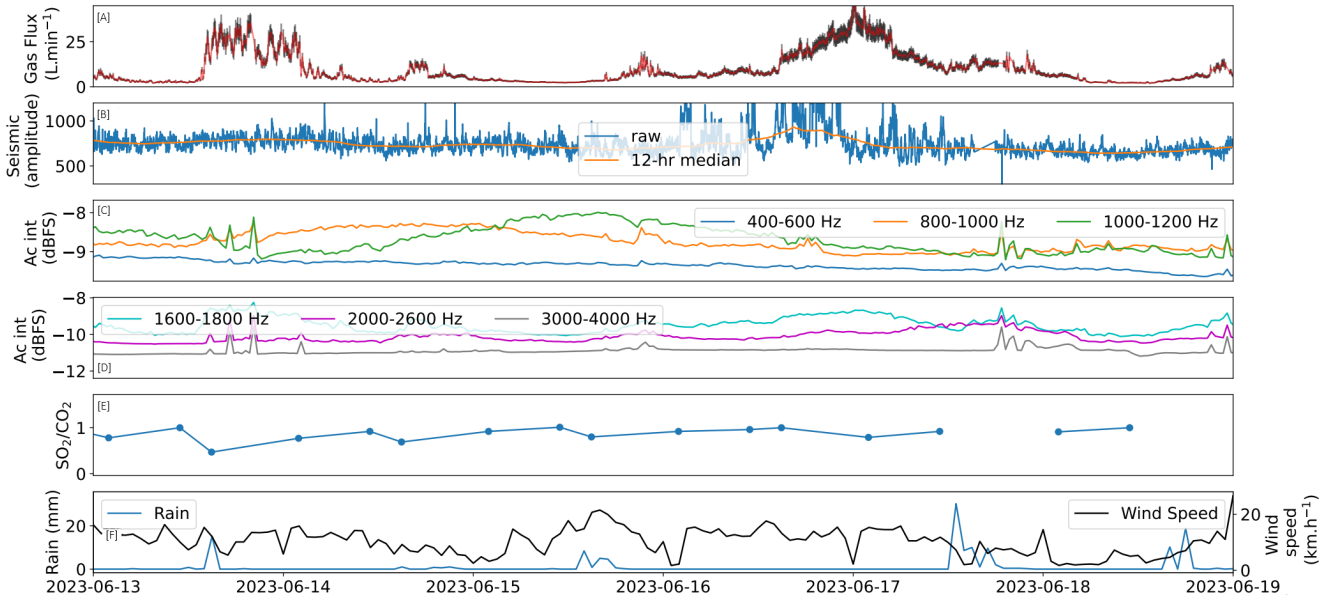

Figure 5: Overview of acoustic, seismic, and chemical results for the mass bubbling period: observations from the mass bubbling period June 13th to 19th. [A] The flux inversion results produced based on hydroacoustic data. [B] The seismic amplitude recorded at a local station. Note the correlation between increasing seismic amplitude and gas flux for the 2nd mass bubbling event. [C–D] The intensity of different acoustic bands as observed in the lake. Spilt split between low (<1500 Hz) and high frequency (>1500 Hz). Note the spikes correlate with rainfall events and are discounted from flux estimates [E] Subaerial gas plume SO_2/CO_2 mixing ratios from MultiGAS. [F] the local rainfall (blue) and windspeed (black) data.

The seismic amplitude appears to gradually increase for the first two days before beginning to gradual decrease. A rapid decrease in seismic amplitude is seen late on the 22nd followed by another period of gradual increasing then decreasing.

The MultiGAS data for this period again show no major changes in gas composition compared to the other periods. The average SO_2/CO_2 ratio was 0.97 ± 0.27 and the H_2S/SO_2 remained near zero. We note, however a significant gap in the recorded data between the 20th and 23rd.

4 Discussion

4.1 Weather acoustics

Although wind speeds did increase progressively throughout the period of observation, they never rose sufficiently high (>30 km hr^{-1}) to produce breaking waves which would create bubbles at the water's surface and complicate the flux inversion process [Nystuen 1986; Wang et al. 2016; Roche 2023]. This notion is further strengthened by the fact that the weather station was on the flank of the volcano not inside the sheltered crater where speeds can be presumed to be even lower.

A strong correlation can be seen between high rainfall events and sudden spikes in the intensity of high frequency signals (>1600 Hz). The weather station recorded high rainfall (>5 mm hr^{-1}) for a total of 29 (out of 600) hours. This is when the rainfall rate is sufficiently high to create bubbles at the surface of the water with enough intensity to interfere with the inversion process [Roche 2023]. The flux inversion process will falsely attribute these surface rainfall bubbles to the volcanic seeps. Fortunately, these rainfall events are short, only four lasting longer than a single hour, meaning their impact is severely reduced by the 3-hour running mean and hence ultimately no anomalous gas flux spikes were caused by rainfall. Future studies would benefit from recording weather conditions directly next to the crater lake.

4.2 Waterfall acoustics

A dozen broad-spectrum acoustic events were observed in the hydroacoustic data throughout this study (see Supplementary Material 1 Figure S6), where the intensity of the acoustic signal suddenly increased across all frequencies for anywhere between 30 s and 20 minutes before abruptly returning to earlier levels. These events were automatically flagged due to the sudden increase in gas flux as measured by the inversion process. Following an audible examination, they were recognised as the sounds of bubble generation and flowing water. Crucially they all occurred following a period of rainfall. Examining webcam videos of the crater during these events we see rainwater flowing over a ledge and into the lake (See Supplementary Material 1 Figure S7). We thus conclude that these sounds are the result of temporary waterfalls forming in the crater, i.e. the sound of water droplets impacting the surface of the lake which are recorded by our hydrophones. As these bubbles are non-volcanic in origin, these time periods are excluded and thus do not affect our gas flux estimates. They do, however, appear in the frequency intensity band graphs.

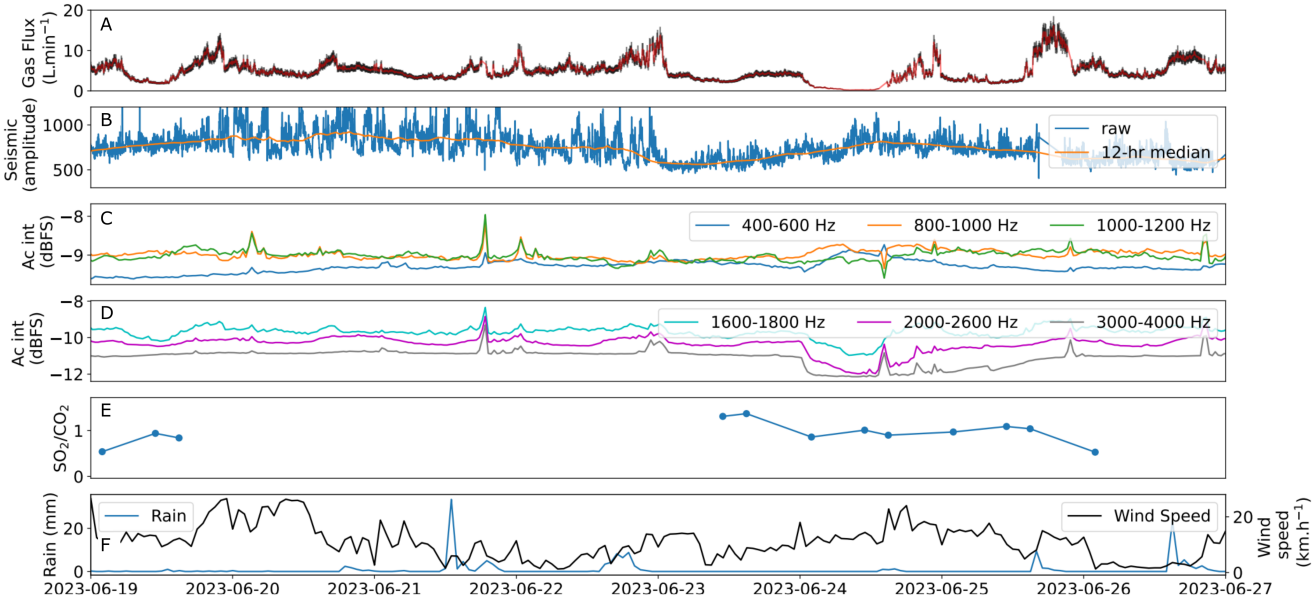

Figure 6: Overview of acoustic, seismic, and chemical results for the post mass bubbling period. Observations from the post mass bubbling period June 19th to 27th [A] The flux inversion results produced based on hydroacoustic data. [B] Seismic observations. [C–D] The intensity of different acoustic bands as observed in the lake spilt split between low (<1500 Hz) and high frequency (>1500 Hz). Note the spikes in frequency bands correlate with rainfall events and are discounted from flux estimates. [E] subaerial gas sampling results. [F] the local rainfall (blue) and windspeed (black) data.

4.3 Sensitivity to overall gas emissions

Based on hydrophone data, gas flux estimates from seeps range from 0.2 ± 0.1 L min^{-1} to 49.0 ± 5.0 L min^{-1}, which can be compared to gas flux estimates from more traditional gas monitoring. At atmospheric pressure and 50 °C water temperature, these volumes equate to approximately 2–2000 moles of gas released per day. If this gas was pure SO_2, then these fluxes would correspond to 0.00013 T d^{-1} to 0.13 T d^{-1} of SO_2. Considering that the SO_2/CO_2 ratio of the gas was ~1 during the observation period, and that at 50 °C water is well below boiling point, the gas would be dominated by SO_2 and CO_2 in roughly equal proportions. Therefore, gas fluxes registered by the hydrophone are equivalent to <0.07 T d^{-1} of SO_2. In comparison, sulfur dioxide fluxes measured at a DOAS station downwind of the volcano were between 55 and 295 T d^{-1} of SO_2 (see de Moor et al. [2019] for methods) during the hydrophone deployment. Therefore, it is clear that the hydrophone data dominantly captures bubbling near the sensor, whereas the main degassing vents were located outside of the hydrophone's range. By this estimation the hydrophone measurement has accounted for the total gas emissions between 28 and 160 m from its mooring (Figure 1). Many potential applications of the hydrophone technique can be envisioned to complement traditional gas monitoring methods. For example, there are multiple degassing sources at Poás, and it is impossible to derive fluxes from individual point sources with DOAS techniques. Hydroacoustics could be the key to quantifying relative contributions from individual seeps which could provide fresh insight into the flow of volatiles beneath the surface. Furthermore, future studies aiming to quantify the entirety of the gas flux from a lake should aim to deploy multiple hydrophones, in the centre of each seep field, in some kind of array around the lake or using distributed acoustic sensors to ensure all bubble sound sources are detected.

4.4 Fumarole acoustics

Non bubble noise was identified in the lake between 400 and 1300 Hz, with the signal generally being strongest between 800 and 1200 Hz. The intensity of this signal varies over time, most notably increasing during the mass bubbling period (Figure 5C). We suspect, but cannot say definitively, that this sound is the result of the subaerial fumaroles that are continuously active in Poás crater, venting volcanic gas directly into the atmosphere. Prior studies have examined very low frequency (<20 Hz) acoustic emissions from fumaroles using infrasound and seismic sensors, demonstrating a decent correlation between their intensity and flux [Gunawan et al. 2016; McKee et al. 2017; Giudicepietro et al. 2019]. There does not however appear to be any detailed analysis of higher frequency (>100 Hz) sounds from fumaroles, in particular as perceived underwater, nor how these correlate to gas emissions. We postulate based on our observations here that it may be possible to empirically map the relationship between fumarole gas flux and subaqueous acoustics and use this to measure future gas emissions. However, one would first need to prove definitively that the fumarole is being heard.

4.5 Diurnal variation

A clear diurnal variation in the intensity of signals between 1600 and 3000 Hz is seen almost throughout the entirety of

this study. This translates to an even clearer diurnal variation in the estimated gas flux, particularly during the initial steady-state period. There is no correlation between diurnal gas flux variations and seismic activity (Figure 7). Diurnal variations in gas flux are not uncommon. It is often seen in the marine environment as a result of hydrostatic pressure (tidal) changes or in peat bogs and lakes as a result of changes in atmospheric pressure [Tokida et al. 2007; Roche 2021]. As there are no tidal variations in the crater lake, we attribute these diurnal variations to changes in atmospheric pressure.

Throughout the day, the area around the lake is heated by the sun. Warm air rises creating a low-pressure system over the lake; this decrease in pressure allows gas to more easily escape from the sediment beneath the lake and thus gas flux increases. The low-pressure system is likely further strengthened by increasing humidity [Vallero 2024]. During the evening as it becomes darker, the area above the lake cools, creating a high-pressure system. The increase in pressure makes it harder for gas to escape from the sediment beneath the lake and thus gas flux decreases (Figure 8). This cycle repeats each day [Roche 2021], barring any major meteorological changes, and is independent of the underlying volcanic activity. Essentially one could imagine the atmospheric pressure acting as a small-scale regulator on the natural volcanic emissions, varying the rate of release. Unfortunately, the local weather station did not record atmospheric pressure, so we are currently unable to state with absolute certainty that this is the cause. However, given that this is a known phenomenon in other nontidal sites [Tokida et al. 2007] and the fact that there is no corresponding diurnal signal in the seismic data (both in terms of seismic amplitude and spectral width), it seems unlikely the variation is driven by volcanic activity.

4.6 Gas flux and seismic activity

As seen in Figure 7, the first mass bubbling event, an order of magnitude increase in gas, does not correlate with any change in seismic activity. Meanwhile the second mass bubbling event correlates strongly with an increase in seismic activity but shows no major change in gas ratios. The most obvious questions that arise from these observations are: 1) What triggered the excess flow of volatiles in each event? 2) Why are there two mass bubbling events so different?

4.6.1 *Aseismic mass bubbling event*

Given the lack of correlation with seismic activity it may be logical to assume the first mass bubbling event is unrelated to volcanic processes. This is not to say the gas is not in some way related to volcanic degassing, indeed this has already been demonstrated [de Moor et al. 2019], but rather that we are witnessing a release from some secondary storage site. Gas pockets are commonly found in marine and lacustrine sediments where gas flow naturally occurs [Boudreau et al. 2005; Algar et al. 2011; Roche et al. 2021; Terzariol et al. 2021]. While there are no direct reports of gas pockets beneath active crater lakes there is no reason to believe they cannot exist and indeed their existence is necessary to explain some seismic observations [Girona et al. 2019; Ardid et al. 2023]. The presence of gas pockets within the sediment of Poás crater lake would serve to further explain the diurnal gas flux variation. The outflow of volatiles from underground being temporarily stored within the sediment from which it is released into the water column is regulated by the overlying pressure conditions (hydrostatic and atmospheric pressure).

While rarely directly observed, gas pockets are known to sometimes expel their contents in a similar fashion to that seen here [Marcon et al. 2019; Gupta et al. 2022; Vaknin et al. 2023]. The expulsion occurs when the sediment trap is no longer capable of containing the gas within it. While there is some debate as to the causes of these expulsion events, generally accepted reasons include changes in the overburden (e.g. storm events altering overlying sediment), exceeding the reservoir capacity, or some form of seal failure (e.g. a rupture forming in the overlying less-permeable layer) [Tary et al. 2012; Andreassen et al. 2017; Marcon et al. 2019; Gupta et al. 2022; Vaknin et al. 2023]. As no strong meteorological or seismic activity is witnessed prior to the start of the event we dismiss the possibility of overburden changes or seal failure (resulting from seismic activity) triggering this event. While it is possible for seals to fail aseismically a trigger is still required which in this instance could only be the addition of more gas. This would suggest the first mass bubbling event is a result of gas pocket(s) under Poás crater lake reaching maximum capacity and rapidly expelling their contents (Figure 8). This would also explain the sudden nature of the first mass bubbling event, especially when compared to the second.

The occurrence of aseismic mass bubbling events could be a useful tool for monitoring volcanic activity. If such events continue to occur at regular intervals, it would be indicative of a steady flow of gas from the underlying magmatic body, into the sediment and then the lake. If the period between aseismic mass bubbling events decreases dramatically it would indicate a sudden increase in the rate of volatiles being released and, potentially, an increase in the volcanic activity. Alternatively, if an extended period of time goes without an aseismic mass bubbling event it may indicate that volatiles are being trapped beneath the surface, increasing the chance of a violent eruption.

Testing this theory would require demonstrating the existence of gas pockets in sediment and observing some cyclicity in the occurrence of these events. Such features are usually only visible via high-frequency seismic surveying and researchers may be hesitant to place such expensive equipment in acidic conditions. Performing such a survey in Poás would allow the presence of gas pockets to be confirmed. Repeated surveys either side of an mass bubbling event could detect any potential change in their size. Until this is achieved such a physical mechanism remains speculative.

4.6.2 *Seismic mass bubbling event*

The second mass bubbling event shows a clear correlation with seismic activity. With a Pearson correlation coefficient at the time of the event of ~0.5 (Figure 7C). Both gas flux and seismic amplitude begin increasing at approximately the same time, around midday on the 15th, and begin decreasing at the same time, around midnight on the 16th. This could be an indication of increased hydrothermal activity or magmatic ac-

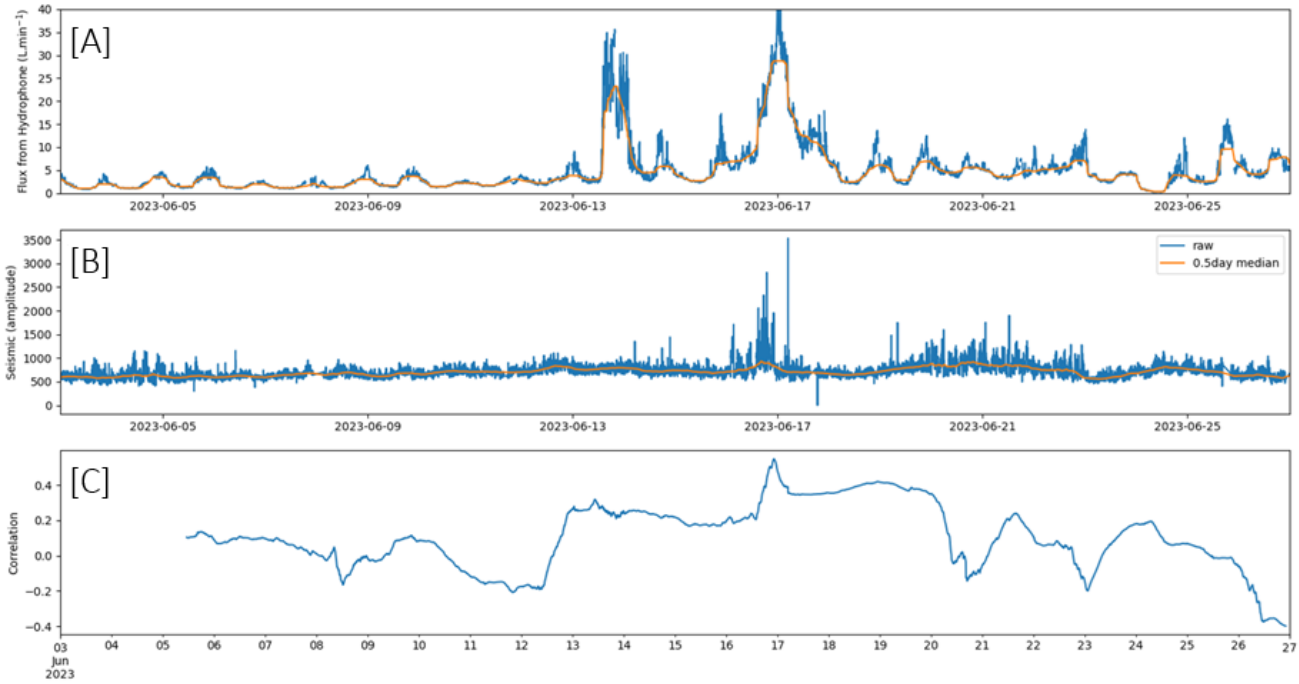

Figure 7: Comparison of flux and seismic measurements across the study period. Observations from the whole period, June 3rd to 27th. [A] The flux inversion results produced based on hydroacoustic data. [B] The seismic amplitude at a local station [C] The Pearson correlation coefficient between seismic amplitude and gas flux.

tivity beneath the crater lake releasing excess volatiles (Figure 8). The increase in the number of short-tremor events appears to precede the gas flux by ~6 hours. It is not possible at this stage to determine the exact physical mechanisms behind this relationship, i.e. is the mass movement of volatiles increasing the seismic activity or did the increased seismic activity simply allow for a greater flow of gas via ruptured seals. However, that a positive relationship exists is highly encouraging and suggests a strong potential for future insight into the inner workings of volcanoes through further study of this topic.

Unfortunately, in this instance no phreatic eruptions were recorded at the surface, but it is highly likely that a future study that does observe an eruption will see a noticeable change in subaquatic gas flux. Here it is important to consider that the observation period took place during a slow increase in volcanic activity at Poás, including increasing SO_2/CO_2 and SO_2 fluxes from minima in late 2021–early 2022 of <0.5 and <100 T d^{-1} to maxima in early 2024 of SO_2/CO_2 >2 and SO_2 fluxes frequently >300 T d^{-1} that coincided with eruptive activity, including explosive eruptions and ash emissions. Thus, the observed increases in bubbling likely represent a portion of the reactivation process.

4.6.3 *Minimal release period*

A notable decrease in seismic activity during the post-mass bubbling period is followed by a similarly large decrease in gas flux with a ~24 hour delay, with the lowest gas flux, 0.2 ± 0.1 L min^{-1}, occurring roughly one day after the lowest mean seismic amplitude. This observation serves to strengthen the notion that gas flux and seismic activity are positively correlated. The apparent lag between them potentially provides some insight into flow of volatiles within the body of the volcano.

5 Conclusions

This study used hydroacoustic data recorded by a single hydrophone in the warm hyperacid crater lake atop Poás Volcano to measure the subaqueous release of volcanic gas over the course of one month. The use of passive acoustic inversion techniques allowed us to measure the volume of gas being released from the lakebed at a sample rate of 5 min, far higher than traditional sub aerial gas sampling techniques. This allowed us to study the temporal variably of seeps at a level far beyond that previously seen, and over an extended period of time.

The large size of the lake combined with restrictions of a singular hydrophone meant we were unable to quantify the total lakebed emissions. Indeed, simultaneous subaerial measurements suggest we only accounted for emissions within 28–160 m of the hydrophone. Future studies could address this limitation with the use of multiple hydrophones in an array around the lake or perhaps using distributed acoustic sensors.

Studying variations in gas emissions from the surveyed portion of the lakebed provided fresh insight into the migration of volatiles within the subsurface. Firstly, we see small-scale diurnal variations of ~2 L min^{-1} driven by local atmospheric pressure conditions. While this appears to be the first observation of day/night gas emission cycles in a volcanic lake, such systems are commonly seen in peat bogs and shallow lakes around the world. In essence, the atmospheric pressure

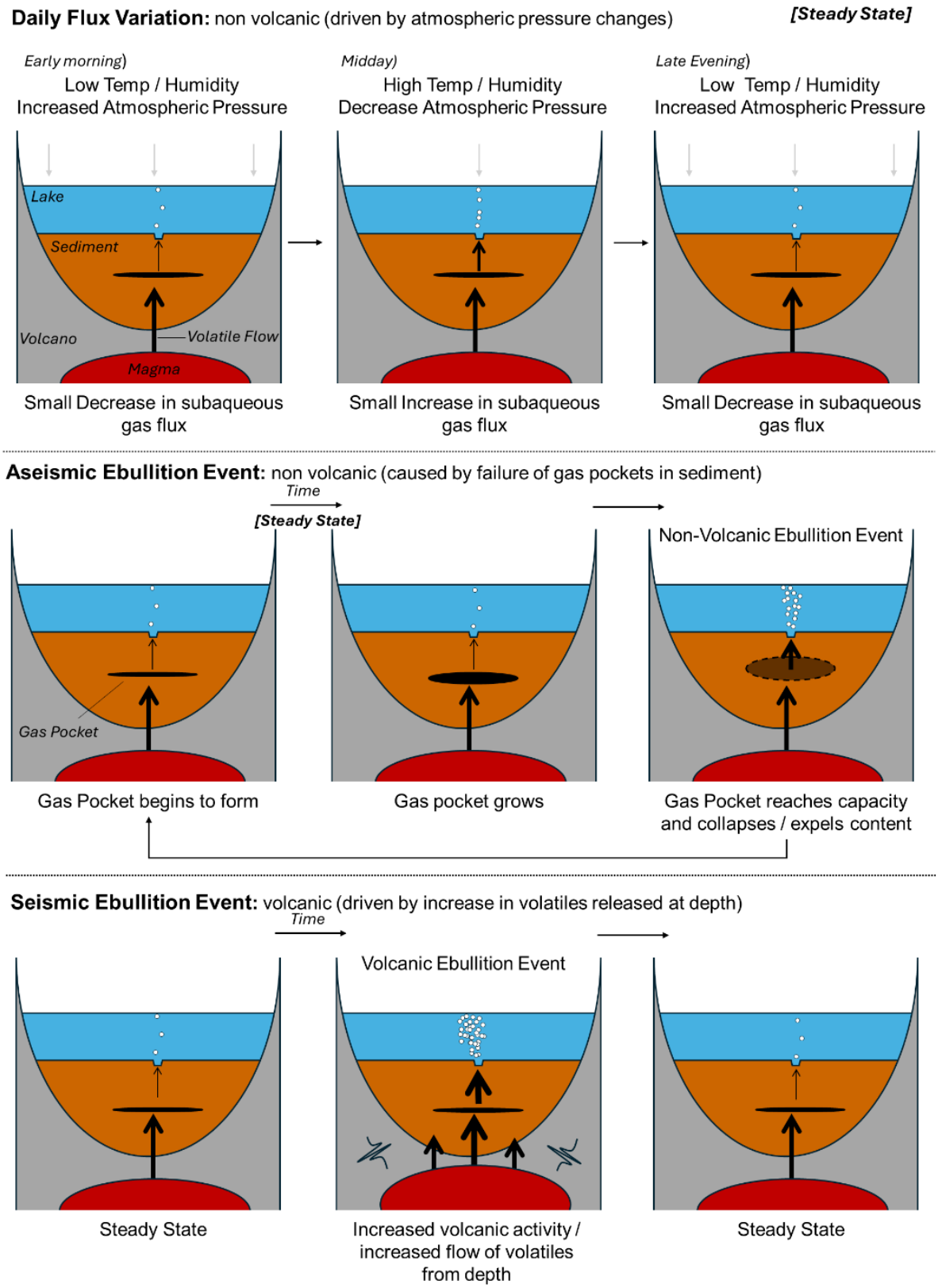

Figure 8: Illustrations of the different events driving flux variation in the lake a diagram demonstrating the different factors driving variations in sub aqueous gas flux in Poás crater lake. Aseismic causes include daily variations due to atmospheric pressure changes and large mass bubbling events caused by the collapse of gas pockets. Seismic events include large mass bubbling events caused as excess volatiles are released from depth.

acts as a small-scale regulator on the natural volcanic emissions into the lake, varying the rate of release. Secondly, we report a large and abrupt aseismic mass bubbling event releasing 18,000 ± 3000 L of gas in just 15 hours (compared to a daily average of 3600 ± 500 L), likely resulting from the collapse of gas pocket(s) in the sediment underlying the lake. Given the lack of other likely triggers we suspect this collapse was triggered by the pocket(s) reaching maximum capacity.

Finally, and most excitingly for volcanic monitoring purposes, we also observe an even larger mass bubbling event releasing 30,000 ± 5000 L of gas in 24 hours. This event was correlated with an increase in local seismic activity and preceded a new eruptive period in the following weeks. We presume this mass bubbling event was the result of excess volatiles being released from deeper within the volcano. These observations combine to form good evidence that a relationship between subaqueous gas flux and volcanic activity exists and could be used as a monitoring tool. While a phreatic eruption was not observed during this period it seems highly likely, based on our observations, that such an event would be telegraphed in hydroacoustic recordings ahead of infrasound observations.

Author Contributions

Conceptualization: BR, CC; Methodology: BR,CC, LL; Acoustic Analysis: BR, JG; Seismic Analysis: CC, LL, HB, JP; Gas Analysis: MdM, AR; Supervision: CC, JP; Writing—original draft: BR; Writing—review & editing: BR, CC, LL, MdM, GA, JP, BH, JG, AR

Acknowledgements

We would like to thank the team at OSCIVORI for all their support facilitating this field work and providing much needed insight. The hydrophone SNAP was borrowed from ISTerre (Grenoble, France) and brought by Alain Bernard to Costa Rica. Weather station data was generously provided by the Instituto Meteorologico Nacional (IMN) of Costa Rica. We acknowledge a FNRS MIS funding entitled CalderaSounds.

Data Availability

Acoustic data from this study is available upon request from Dr. Ben Roche. Seismic and chemical data from this study is available via OVSICORI-UNA. Weather station data is available upon request from National Metrological Institute (IMN) of Costa Rica.

Copyright notice

References

Algar, C. K., B. P. Boudreau, and M. A. Barry (2011). "Initial rise of bubbles in cohesive sediments by a process of viscoelastic fracture". *Journal of Geophysical Research* 116(B4). DOI: 10.1029/2010jb008133.

Andreassen, K., A. Hubbard, M. Winsborrow, H. Patton, S. Vadakkepuliyambatta, A. Plaza-Faverola, E. Gudlaugsson, P. Serov, A. Deryabin, R. Mattingsdal, J. Mienert, and S. Bünz (2017). "Massive blow-out craters formed by hydrate-controlled methane expulsion from the Arctic seafloor". *Science* 356(6341), pages 948–953. DOI: 10.1126/science.aal4500.

Ardid, A., D. Dempsey, C. Caudron, S. J. Cronin, C. A. Miller, I. Melchor, D. Syahbana, and B. Kennedy (2023). "Using Template Matching to Detect Hidden Fluid Release Episodes Beneath Crater Lakes in Ruapehu, Copahue, and Kawah Ijen Volcanoes". *Journal of Geophysical Research: Solid Earth* 128(10). DOI: 10.1029/2023jb026729.

Bayrakci, G. and F. Klingelhoefer, editors (2023). Wiley. 268 pages. ISBN: 9781119750925. DOI: 10.1002/9781119750925.

Bergès, B. J., T. G. Leighton, and P. R. White (2015). "Passive acoustic quantification of gas fluxes during controlled gas release experiments". *International Journal of Greenhouse Gas Control* 38, pages 64–79. DOI: 10.1016/j.ijggc.2015.02.008.

Boudreau, B. P., C. Algar, B. D. Johnson, I. Croudace, A. Reed, Y. Furukawa, K. M. Dorgan, P. A. Jumars, A. S. Grader, and B. S. Gardiner (2005). "Bubble growth and rise in soft sediments". *Geology* 33(6), pages 517–520. DOI: 10.1130/g21259.1.

Caliro, S., A. Caracausi, G. Chiodini, M. Ditta, F. Italiano, M. Longo, C. Minopoli, P. M. Nuccio, A. Paonita, and A. Rizzo (2004). "Evidence of a recent input of magmatic gases into the quiescent volcanic edifice of Panarea, Aeolian Islands, Italy". *Geophysical Research Letters* 31(7). DOI: 10.1029/2003gl019359.

Caudron, C., A. Mazot, and A. Bernard (2012). "Carbon dioxide dynamics in Kelud volcanic lake". *Journal of Geophysical Research: Solid Earth* 117(B5). DOI: 10.1029/2011jb008806.

Caudron, C., J. Vandemeulebrouck, and R. A. Sohn (2022). "Turbulence-induced bubble nucleation in hydrothermal fluids beneath Yellowstone Lake". *Communications Earth & Environment* 3(1). DOI: 10.1038/s43247-022-00417-6.

Chiodini, G., A. Paonita, A. Aiuppa, A. Costa, S. Caliro, P. De Martino, V. Acocella, and J. Vandemeulebrouck (2016). "Magmas near the critical degassing pressure drive volcanic unrest towards a critical state". *Nature Communications* 7(1). DOI: 10.1038/ncomms13712.

D'Arcy, F., J. M. de Moor, J. Stix, A. Alan, R. Bogue, E. Corrales, J. A. Diaz, E. Mick, J. Salas-Navarro, and R. Lauzeral (2022). "New insights into carbon isotope systematics at Poás volcano, Costa Rica". *Journal of Volcanology and Geothermal Research* 431, page 107639. DOI: 10.1016/j.jvolgeores.2022.107639.

Deane, G. B. and M. D. Stokes (2008). "The acoustic excitation of air bubbles fragmenting in sheared flow". *The Journal of the Acoustical Society of America* 124(6), pages 3450–3463. DOI: 10.1121/1.3003076.

De Moor, J. M., J. Stix, G. Avard, C. Muller, E. Corrales, J. A. Diaz, A. Alan, J. Brenes, J. Pacheco, A. Aiuppa, and T. P. Fischer (2019). "Insights on Hydrothermal-Magmatic Interactions and Eruptive Processes at Poás Volcano (Costa Rica) From High-Frequency Gas Monitoring and Drone Measurements". *Geophysical Research Letters* 46(3), pages 1293–1302. DOI: 10.1029/2018gl080301.

De Moor, J., A. Aiuppa, J. Pacheco, G. Avard, C. Kern, M. Liuzzo, M. Martínez, G. Giudice, and T. Fischer (2016). "Short-period volcanic gas precursors to phreatic eruptions: Insights from Poás Volcano, Costa Rica". *Earth and Planetary Science Letters* 442, pages 218–227. DOI: 10.1016/j.epsl.2016.02.056.

Etiope, G. and S. Schwietzke (2019). "Global geological methane emissions: An update of top-down and bottom-up estimates". *Elementa: Science of the Anthropocene* 7 (47). DOI: 10.1525/elementa.383.

Girona, T., C. Caudron, and C. Huber (2019). "Origin of Shallow Volcanic Tremor: The Dynamics of Gas Pockets Trapped Beneath Thin Permeable Media". *Journal of Geophysical Research: Solid Earth* 124(5), pages 4831–4861. DOI: 10.1029/2019jb017482.

Giudicepietro, F., G. Chiodini, S. Caliro, W. De Cesare, A. M. Esposito, D. Galluzzo, D. Lo Bascio, G. Macedonio, M. Orazi, P. Ricciolino, and J. Vandemeulebrouck (2019). "Insight Into Campi Flegrei Caldera Unrest Through Seismic Tremor Measurements at Pisciarelli Fumarolic Field". *Geochemistry, Geophysics, Geosystems* 20(11), pages 5544–5555. DOI: 10.1029/2019gc008610.

Gunawan, H., C. Caudron, J. Pallister, S. Primulyana, B. Christenson, W. Mccausland, V. van Hinsberg, J. Lewicki, D. Rouwet, P. Kelly, C. Kern, C. Werner, J. B. Johnson, S. B. Utami, D. K. Syahbana, U. Saing, Suparjan, B. H. Purwanto, C. Sealing, M. M. Cruz, S. Maryanto, P. Bani, A. Laurin, A. Schmid, K. Bradley, I. G. M. A. Nandaka, and M. Hendrasto (2016). "New insights into Kawah Ijen's volcanic system from the wet volcano workshop experiment". *Geological Society, London, Special Publications* 437(1), pages 35–56. DOI: 10.1144/sp437.7.

Gupta, S., C. Schmidt, C. Böttner, L. Rüpke, and E. H. Hartz (2022). "Spontaneously Exsolved Free Gas During Major Storms as an Ephemeral Gas Source for Pockmark Formation". *Geochemistry, Geophysics, Geosystems* 23(8). DOI: 10.1029/2021gc010289.

Haris, K., N. Shajahan, B. Bergès, and R. J. Kloser (2023). "Evaluation of passive acoustic methods for ambient noise baseline and gas flow rate quantification at a proposed nearshore carbon capture and storage site in Australia". *International Journal of Greenhouse Gas Control* 129, page 103961. DOI: 10.1016/j.ijggc.2023.103961.

Leifer, I. and R. K. Patro (2002). "The bubble mechanism for methane transport from the shallow sea bed to the surface: A review and sensitivity study". *Continental Shelf Research* 22(16), pages 2409–2428. DOI: 10.1016/s0278-4343(02)00065-1.

Leighton, T. G. (1994). "The Freely-oscillating Bubble". *The Acoustic Bubble*. Edited by T. G. Leighton. Elsevier. Chapter 3, pages 129–286. ISBN: 9780124419209. DOI: 10.1016/b978-0-12-441920-9.50008-0.

Leighton, T. G. and P. R. White (2011). "Quantification of undersea gas leaks from carbon capture and storage facilities, from pipelines and from methane seeps, by their acoustic emissions". *Proceedings of the Royal Society A: Mathematical, Physical and Engineering Sciences* 468(2138), pages 485–510. DOI: 10.1098/rspa.2011.0221.

Li, J., B. Roche, J. M. Bull, P. R. White, J. W. Davis, M. Deponte, E. Gordini, and D. Cotterle (2020a). "Passive acoustic monitoring of a natural CO2 seep site – Implications for carbon capture and storage". *International Journal of Greenhouse Gas Control* 93, page 102899. DOI: 10.1016/j.ijggc.2019.102899.

Li, J., B. Roche, J. M. Bull, P. R. White, T. G. Leighton, G. Provenzano, M. Dewar, and T. J. Henstock (2020b). "Broadband Acoustic Inversion for Gas Flux Quantification—Application to a Methane Plume at Scanner Pockmark, Central North Sea". *Journal of Geophysical Research: Oceans* 125(9). DOI: 10.1029/2020jc016360.

Li, J., P. R. White, B. Roche, J. M. Bull, T. G. Leighton, J. W. Davis, and J. W. Fone (2021). "Acoustic and optical determination of bubble size distributions – Quantification of seabed gas emissions". *International Journal of Greenhouse Gas Control* 108, page 103313. DOI: 10.1016/j.ijggc.2021.103313.

Longo, M., G. Lazzaro, C. G. Caruso, A. Corbo, S. Sciré Scappuzzo, F. Italiano, A. Gattuso, and D. Romano (2021). "Hydro-acoustic signals from the Panarea shallow hydrothermal field: new inferences of a direct link with Stromboli". *Geological Society, London, Special Publications* 519(1), pages 59–74. DOI: 10.1144/sp519-2020-184.

Maeck, A., H. Hofmann, and A. Lorke (2014). "Pumping methane out of aquatic sediments – ebullition forcing mechanisms in an impounded river". *Biogeosciences* 11(11), pages 2925–2938. DOI: 10.5194/bg-11-2925-2014.

Makarov, M. M., S. I. Muyakshin, K. M. Kucher, I. A. Aslamov, and N. G. Granin (2020). "A study of the gas seep Istok in the Selenga shoal using active acoustic, passive acoustic and optical methods". *Journal of Great Lakes Research* 46(1), pages 95–101. DOI: 10.1016/j.jglr.2019.10.014.

Mannich, M., C. V. S. Fernandes, and T. B. Bleninger (2019). "Uncertainty analysis of gas flux measurements at air–water interface using floating chambers". *Ecohydrology & Hydrobiology* 19(4), pages 475–486. DOI: 10.1016/j.ecohyd.2017.09.002.

Marcon, L., T. Bleninger, M. Männich, and S. Hilgert (2019). "High-frequency measurements of gas ebullition in a Brazilian subtropical reservoir—identification of relevant triggers and seasonal patterns". *Environmental Monitoring and Assessment* 191(6). DOI: 10.1007/s10661-019-7498-9.

Martínez-Bazán, C., J. L. Montañés, and J. C. Lasheras (1999). "On the breakup of an air bubble injected into a fully developed turbulent flow. Part 1. Breakup frequency". *Journal of Fluid Mechanics* 401, pages 157–182. DOI: 10.1017/s0022112099006680.

McGinnis, D. F., J. Greinert, Y. Artemov, S. E. Beaubien, and A. Wüest (2006). "Fate of rising methane bubbles in strati-

fied waters: How much methane reaches the atmosphere?" *Journal of Geophysical Research: Oceans* 111(C9). DOI: 10.1029/2005jc003183.

McKee, K., D. Fee, A. Yokoo, R. S. Matoza, and K. Kim (2017). "Analysis of gas jetting and fumarole acoustics at Aso Volcano, Japan". *Journal of Volcanology and Geothermal Research* 340, pages 16–29. DOI: 10.1016/j.jvolgeores.2017.03.029.

Nystuen, J. A. (1986). "Rainfall measurements using underwater ambient noise". *The Journal of the Acoustical Society of America* 79(4), pages 972–982. DOI: 10.1121/1.393695.

Qi, Y., A. U. Mohammad Masuk, and R. Ni (2020). "Towards a model of bubble breakup in turbulence through experimental constraints". *International Journal of Multiphase Flow* 132, page 103397. DOI: 10.1016/j.ijmultiphaseflow.2020.103397.

Razaz, M., D. Di Iorio, B. Wang, S. Daneshgar Asl, and A. M. Thurnherr (2020). "Variability of a natural hydrocarbon seep and its connection to the ocean surface". *Scientific Reports* 10(1). DOI: 10.1038/s41598-020-68807-4.

Roche, B. (2021). "Methods for determining gas flux within the water column". PhD thesis. University of Southampton.

– (2023). "Ambient Bubble Acoustics – Seep, Rain and Wave Noise". *Noisy Oceans: Monitoring Seismic and Acoustic Signals in the Marine Environment*. Edited by G. Bayrakci and F. Klingelhoefer. Wiley. Chapter 10, pages 161–182. ISBN: 9781119750925. DOI: 10.1002/9781119750925.ch10.

Roche, B., J. M. Bull, H. Marin-Moreno, T. G. Leighton, I. H. Falcon-Suarez, M. Tholen, P. R. White, G. Provenzano, A. Lichtschlag, J. Li, and M. Faggetter (2021). "Time-lapse imaging of CO2 migration within near-surface sediments during a controlled sub-seabed release experiment". *International Journal of Greenhouse Gas Control* 109, page 103363. DOI: 10.1016/j.ijggc.2021.103363.

Roche, B., P. R. White, J. M. Bull, T. G. Leighton, J. Li, C. Christie, and J. Fone (2022). "Methods of acoustic gas flux inversion—Investigation into the initial amplitude of bubble excitation". *The Journal of the Acoustical Society of America* 152(2), pages 799–806. DOI: 10.1121/10.0013220.

Rouwet, D., L. Sandri, W. Marzocchi, J. Gottsmann, J. Selva, R. Tonini, and P. Papale (2014). "Recognizing and tracking volcanic hazards related to non-magmatic unrest: a review". *Journal of Applied Volcanology* 3(1). DOI: 10.1186/s13617-014-0017-3.

Salvage, R. O., G. Avard, J. M. de Moor, J. F. Pacheco, J. Brenes Marin, M. Cascante, C. Muller, and M. Martinez Cruz (2018). "Renewed Explosive Phreatomagmatic Activity at Poás Volcano, Costa Rica in April 2017". *Frontiers in Earth Science* 6. DOI: 10.3389/feart.2018.00160.

Tary, J. B., L. Géli, C. Guennou, P. Henry, N. Sultan, N. Çağatay, and V. Vidal (2012). "Microevents produced by gas migration and expulsion at the seabed: a study based on sea bottom recordings from the Sea of Marmara: Microevents produced by gas migration". *Geophysical Journal International* 190(2), pages 993–1007. DOI: 10.1111/j.1365-246x.2012.05533.x.

Terzariol, M., N. Sultan, R. Apprioual, and S. Garziglia (2021). "Pore Habit of Gas in Gassy Sediments". *Journal of Geophysical Research: Solid Earth* 126(5). DOI: 10.1029/2020jb021511.

Tokida, T., T. Miyazaki, M. Mizoguchi, O. Nagata, F. Takakai, A. Kagemoto, and R. Hatano (2007). "Falling atmospheric pressure as a trigger for methane ebullition from peatland". *Global Biogeochemical Cycles* 21(2). DOI: 10.1029/2006gb002790.

Tokoro, T., A. Watanabe, H. Kayanne, K. Nadaoka, H. Tamura, K. Nozaki, K. Kato, and A. Negishi (2007). "Measurement of air–water CO2 transfer at four coastal sites using a chamber method". *Journal of Marine Systems* 66(1–4), pages 140–149. DOI: 10.1016/j.jmarsys.2006.04.010.

Urban, P., M. E. Veloso-Alarcón, and J. Greinert (2023). "Echo grid integration: A novel method for preprocessing multibeam water column data to quantify underwater gas bubble emissions". *Limnology and Oceanography: Methods* 21(7), pages 377–400. DOI: 10.1002/lom3.10552.

Vaknin, I., E. Aharonov, R. Holtzman, and O. Katz (2023). "Gas seepage and pockmark formation from subsurface reservoirs: Insights from table-top experiments". DOI: 10.22541/essoar.170143993.31236316/v1.

Vallero, D. A. (2024). "Water and the atmosphere". *Air Pollution Calculations*. Elsevier, pages 191–223. ISBN: 9780443139871. DOI: 10.1016/b978-0-443-13987-1.00008-9.

Vandemeulebrouck, J., J.-C. Sabroux, M. Halbwachs, Surono, N. Poussielgue, J. Grangeon, and J. Tabbagh (2000). "Hydroacoustic noise precursors of the 1990 eruption of Kelut Volcano, Indonesia". *Journal of Volcanology and Geothermal Research* 97(1–4), pages 443–456. DOI: 10.1016/s0377-0273(99)00176-6.

Vazquez, A., R. Manasseh, and R. Chicharro (2015). "Can acoustic emissions be used to size bubbles seeping from a sediment bed?" *Chemical Engineering Science* 131, pages 187–196. DOI: 10.1016/j.ces.2015.03.058.

Veloso, M., J. Greinert, J. Mienert, and M. De Batist (2019). "Corrigendum: A new methodology for quantifying bubble flow rates in deep water using splitbeam echosounders: Examples from the Arctic offshore NW-Svalbard". *Limnology and Oceanography: Methods* 17(2), pages 177–178. DOI: 10.1002/lom3.10313.

Veloso-Alarcón, M. E., P. Urban, T. Weiss, K. Köser, M. She, and J. Greinert (2022). "Quantitatively Monitoring Bubble-Flow at a Seep Site Offshore Oregon: Field Trials and Methodological Advances for Parallel Optical and Hydroacoustical Measurements". *Frontiers in Earth Science* 10. DOI: 10.3389/feart.2022.858992.

Wang, D. W., H. W. Wijesekera, E. Jarosz, W. J. Teague, and W. S. Pegau (2016). "Turbulent Diffusivity under High Winds from Acoustic Measurements of Bubbles". *Journal of Physical Oceanography* 46(5), pages 1593–1613. DOI: 10.1175/jpo-d-15-0164.1.

Zhu, R., Y. Liu, H. Xu, T. Huang, J. Sun, E. Ma, and L. Sun (2010). "Carbon dioxide and methane fluxes in the littoral zones of two lakes, east Antarctica". *Atmospheric Environment* 44(3), pages 304–311. DOI: 10.1016/j.atmosenv.2009.10.038.